


Hierarchical self-assembling and helical structure in focal conic domains in meniscus of ferroelectric liquid crystal


Amit Choudhary ^{1,*} Suraj Kumar,^{2,3} Ambika Bawa,^{2,3} Surinder P. Singh,^{2,3} Anil K. Thakur ⁴,
Rajesh,^{2,3} and Ashok M. Biradar^{3,†}

¹Physics Department, Deshbandhu College, University of Delhi, Kalkaji, New Delhi-110019, India

²Academy of Scientific and Innovative Research (AcSIR), Ghaziabad-201002, India

³CSIR–National Physical Laboratory, Dr. K. S. Krishnan Marg, New Delhi-110012, India

⁴DIT University, Dehradun, Uttarakhand-248009, India

 (Received 14 June 2021; revised 14 October 2021; accepted 31 March 2022; published 25 April 2022)

We investigate experimentally the formation of focal conic domains of the ferroelectric phase of a liquid crystal, chiral smectic C (SmC^*), in the meniscus geometry. The meniscus geometry is formed in the gap between two glass plates which are placed on a common substrate. This gap is called here a *physical cavity*. Focal conic domains (FCDs) in the physical cavity with dimensions of micrometer scale are investigated under an optical polarizing microscope which enables us to extract the information on the helical structure formation in the constraint and gradient topological meniscus interface. The helical pitch in the FCD is observed to be shorter than in planar confined geometry. A crucial phenomenon of unwrapping and wrapping of helical structure from one FCD to another is also observed. In-plane application of an electric field on a FCD revealed the asymmetric helical unwinding process whereas an increase in temperature has shown symmetrical unwinding. The helical structure based observation is significant for understanding the ferroelectric phase in focal conic domains and their application in microlenses and optical components.

DOI: [10.1103/PhysRevE.105.044706](https://doi.org/10.1103/PhysRevE.105.044706)

I. INTRODUCTION

After the discovery of much required application of liquid crystals (LCs) in displays in the 1970s and later spin-off technologies for compact displays and photonic devices, the interfacial studies of LCs with solids have been extended to decipher the wetting properties of LCs. The meniscus profile of isotropic liquids and LCs in a cavity is governed by parameters such as the thickness of the material film and its molecular interaction with the wall of the capillary [1,2]. Minimization of interaction energy with the boundary walls of a capillary relaxes the mechanical stress and generates various surface-induced textures in the LC, particularly in smectic phase, such as stripes, egg shape, corona, and focal conic domain (FCD) structures. In the smectic C (SmC) phase, the tilting of molecules in the smectic layer originates the striped texture which disappears in the SmA phase [2]. In a freestanding film of the chiral smectic C (SmC^*) phase, also called as ferroelectric phase (FLC), the meniscus surface profile is very crucial due to the fact that the periodicity of stripes increases as the thickness of the film increases according to the surface profile of the meniscus. The dependency of stripes on the thickness of the film and surface-induced molecular tilting of the molecular director in the SmC^* phase is responsible for the striped structure [3,4].

The Focal conic domain is another surface-induced defect structure in smectic LCs which has been studied in detail after its discovery by Friedel. He explained their geometry based on the topological relation with the symmetry of the medium; later it became the broad research field of curvature defects in liquid crystals [5–9]. The focal conic domain is one of the most commonly observed structures in the smectic phases (SmA ; chiral and nonchiral SmC) of LC materials. This structure is even observed in a conventional geometry sample cell. A thin film in SmA , open to air and aligned over the substrate, has revealed a periodic lattice of close packed nontoroidal FCDs. They have high eccentricity with respect to the aligning substrate; such a form of packing is a result of the frustration of the SmA layered structure and anchoring at the aligning substrate [10]. Recently, the hierarchical self-assembly of FCDs in the SmA phase has been observed on the periodic laser ablated undulated (straight and circular patterns) interfacial structure on polydimethylsiloxane (PDMS) in the SmA film in which eccentricity is found to be larger at the extreme height whereas it is the least in the middle portion of the periodic undulated structure [11]. The control over the anchoring energy in the microchannels, carved in the PDMS slab, has resulted in changes in the physical parameters of FCDs such as size, size distribution, and packing structure [12–14]. The homeotropic (vertical) surface anchoring condition of a colloidal dimer in a smectic film has originated a flowerlike texture of FCDs with a larger eccentricity near the colloidal interface than FCDs away from it [15]. An elastic anchoring model of a toric FCD (TFCD) is used to consider the dependence of the radius of the TFCD in the confined

*amitnpl2005@gmail.com

†abiradar.npl@gmail.com

depth of a microchannel of silicon material. TFCDs could also be unstable if the anchoring energy at the substrate is not able to compete with the elastic energy of the curvature [16–19]. Even if the constraint spacing is kept smaller than the critical size, Dupin cyclide structure of FCDs is not formed in SmA in microwrinkle grooves due to the weak anchoring energy of the substrate to overcome the layer bending elastic energy [20]. The anchoring energy is a very crucial parameter for the variation in the size, shape, and even the existence of FCDs in the SmA phase.

Most of the focal conic structural based studies have been associated to the SmA phases. It is quite common to observe FCDs in homogeneously (planar) aligned parallel plate sample cells of the SmC* phase [21–23]. Molecular alignment in the sample cell is controlled by the anchoring energy of the alignment layer and the chiral nature of the SmC* phase where the helical structure of the molecular director is supposed to be formed. In a thin cell of surface stabilized geometry (cell thickness less than the helical pitch value of FLC), no helix is formed. However, in a thicker sample of thickness more than $25\ \mu\text{m}$, helical winding is formed by the wrapped smectic layers in FCDs as shown by polarizing optical microscopy [23]. The wrapping of smectic layers in FCDs of thick samples is shown by x-ray diffraction studies. Smectic layers wrapping about a line of ellipse and hyperbola of FCD are arranged in bookshelf geometry with a slight kink in small FCDs which becomes a normal bookshelf for larger FCDs in the same geometry of the homogeneous alignment condition [24]. The application prospect of FCDs in smectic LCs has been explored in a design of gradient-index microlenses having a focal length in the range of a few micrometers in SmA phases [19,25–27], optical compound lenses [28], and as a lithography mask [29]. Almost all the FCD studies are focused on the development of FCDs in the confined geometry of the sample cell.

In the present study, we have investigated the FCD formation in the SmC* phase in a physical cavity which is open to the air from one side and planarly aligned to the other side by the bottom substrate. The meniscus film is formed on the substrate by confining FLC between the walls of the physical cavity on the aligning substrate. The objective of this study is to obtain insight of the self-assembly of FCDs in a hierarchical manner in the meniscus with the helical structure of the FLC molecular director. In a FCD, smectic layer singularities are formed in ellipse and hyperbola curves about which the smectic layers are wrapped. A hyperbolic singularity curve, passing through the FCD, is ended at the air-FLC interface by passing through the inner structure of the FCD. This end point of hyperbolic singularity is observed as a spot in the FCD texture and is called, in this study, the singularity point. The wave vector of the helical structure is radially outward from the hyperbolic singularity. The helical structure of the FLC molecular director in curved smectic layers inside the FCDs is analyzed in terms of helical pitch in contrast to conventional confined planar geometry. The helical structure and the tilt formation in the meniscus geometry and its dependence on the electric field are studied by optical and electro-optical techniques in the SmC* phase. The FCDs are observed with varying helical pitch, eccentricity, and size of ellipse in FCDs along which the smectic layers are wrapped. A clear linkage

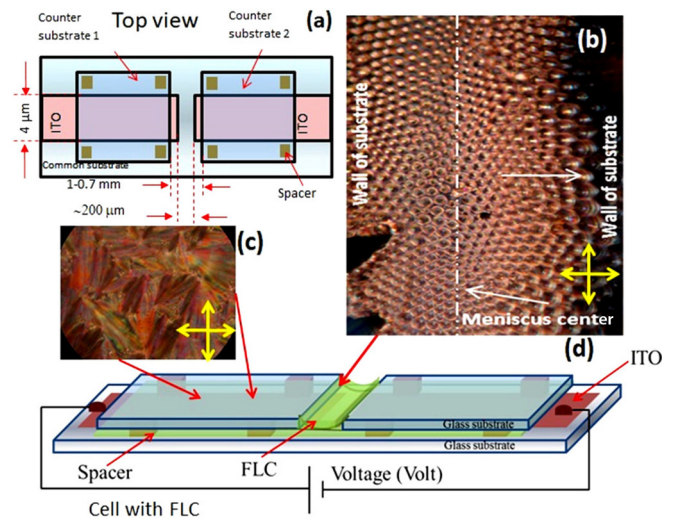


FIG. 1. Schematic representation of the sample setup for the growth of FCDs in FLC material. (a) Top view of the sample geometry without FLC incorporation. (b) Optical texture after incorporated FLC in the physical cavity between two top countersubstrates (1 and 2), showing the growth of the FCD array in FLC. (c) Optical texture of FLC in the confined geometry between the counter- and common substrates. (d) Schematic of the complete sample cell geometry with FLC and electrical connections for applying the dc field. Crossed arrows indicate the position of polarizer and analyzer.

between two neighboring FCDs has been visualized through the layer unwrapping and wrapping phenomenon of helical structure.

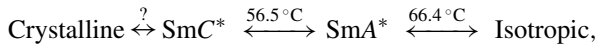
II. EXPERIMENT

The sample is so designed that it shows the two regions in the same sample cell. One region is like a conventional cell having the countersubstrates confining the FLC material. The second region is open to the air from one side and bounds the other side by the glass substrates. This second region is used to obtain the meniscus profile and development of the FCDs therein. The meniscus of the FLC will be confined in the open space between the two countersubstrates (1 and 2) fixed on the common substrate and called physical cavity, as shown in Fig. 1(a). The FCDs of the FLCs were developed in the meniscus of the physical cavity, Fig. 1.

A provision was made for applying an in-plane electric field on the molecules in the FCDs in the meniscus region. This led us to design the two end-to-end facing stripe electrodes on the common substrate (bottom) with requisite specifications. In the current study, highly conducting (sheet resistance $(30 \pm 3)\ \Omega/\square$) and transparent indium tin oxide (ITO) coated glass plates were used as substrates for making the electrodes. A desired two rectangular shape stripe pattern of conducting ITO film was fabricated on the ITO coated glass plates using the photolithography technique. The end-to-end gap between the stripe electrodes was fixed to be $\sim 200\ \mu\text{m}$. The width of each stripe was kept to 4 mm on the bottom substrate. The thickness of the ITO film was around 700–900 Å. The ITO electrode deposited substrate and other countersubstrates (1 and 2, having no ITO coating) were treated with

polymer nylon 6/6 by spin coating before the cell assembly to provide a planar alignment of the FLC molecules in the confined physical cavity. The homogeneous (planar) alignment was obtained by rubbing the countersubstrate (1 and 2) and the common bottom substrate [30]. All the substrates were assembled in the way shown in the schematic diagram of Fig. 1(a). The in-plane gap between the countersubstrates was maintained around 0.7–1 mm which is more than the gap between the ITO electrodes ($\sim 200 \mu\text{m}$). Thus, the meniscus was obtained for the formation of FCDs within the cavity. The spacing between counter- and common substrates was maintained by using Mylar spacers of thickness $14 \mu\text{m}$, Fig. 1(a).

The FLC material LAP-1 [31] was kept in the cell in the physical cavity between two in-plane countersubstrates. Then, the temperature of the FLC material containing cell was achieved 5°C above its isotropic phase (66.4°C) for 30 min at which the isotropic form of the FLC material was injected into the gap between the parallel plates of the cell by means of capillary action and then cooled gradually until reaching room temperature, 28°C . The meniscus was formed over the gap between the two electrodes and between the in-plane countersubstrates (1 and 2). The textures of FLC in the cavity and in one of the confined portions are shown in Figs. 1(b) and 1(c), respectively. Electrical connections were taken out from the ITO electrodes on the common substrate (bottom) for applying the in-plane electric field on the FLC material in cavity. The phase sequence of the used FLC material, LAP-1, is as follows [32]:



where “?” represents the unavailability of the phase transition temperature between two phases. “SmC* and SmA*” are the representation of the chiral smectic C and chiral smectic A phases of the FLC material, respectively. Helical pitch and spontaneous polarization (P_s) values of LAP-1, FLC are $\sim 0.7\text{--}1 \mu\text{m}$ and $\sim 26 \text{ nC/cm}^2$, respectively.

The alignment of FLC molecules in both regions was investigated under a polarizing optical microscope (Carl Zeiss, Axioskop-40A Pol, Germany) with cross polarizers. Electro-optical studies were carried out by applying a dc field using a homemade dc power supply. The temperature of the sample cell for temperature dependent studies was controlled by using a hot stage temperature controller (Julabo F-25 HE, Germany) having a temperature stability precision of $\pm 0.1^\circ\text{C}$.

III. RESULTS AND DISCUSSION

The Results and Discussion section deals with the detailed analysis of the physical structure of the meniscus and FCDs including size, shape, and internal structure of the FCD. The influence of electric field on the internal structure of the FCD in the SmC* phase and the temperature dependent texture analysis has been discussed in a separate section which reveals the existence of concentric rings in the FCD and confirms them as helical structure. The majority of the analysis is performed in the SmC* phase of the LC material. However, in the last section, temperature dependent textural study is carried out in the SmA* phase too.

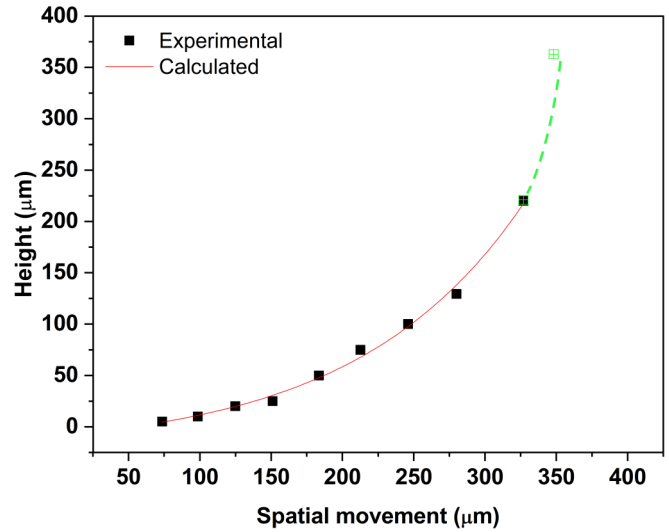


FIG. 2. Height of the meniscus from the common substrate measured experimentally as a function of spatial distance from the middle of the meniscus. The thickness of the FLC film is around $5\text{--}8 \mu\text{m}$ in the middle of the meniscus and varies toward the wall of the physical cavity as measured by focusing the objective lens of the microscope on the FCDs. The fitted line represents the calculated height in which the solid line represents the experimentally observed data fitting by Eq. (1), whereas the dashed line represents the data of extrapolated height at the exact interface of the FLC and solid wall of the cavity by using the Wilhelmy method.

A. Air-FLC interface

As per the sample fabrication scheme, the confined and meniscus geometries are obtained in the single sample as shown in Fig. 1. As can be seen in Fig. 1(b), the FCDs in the meniscus show the ordered distribution, whereas in confined geometry, they have distinct geometrical structure due to confinement by the countersubstrates, Fig. 1(c). The texture in Fig. 1(b) reveals the spatially varying FCD structure within the meniscus. The height of the air-FLC interface is measured using the focus on the texture once at the top surface of the common substrate as a reference point and then at the top of the FCD moving the focus of the objective lens from the middle toward the wall, Fig. 2. This movement of the objective lens of the microscope has resulted in the measurement of the height of the interface at various locations of FCDs in the meniscus. The focus is kept on the FCD where the contrast is very clear. The vertical height is measured with the help of the micrometer scale of a Vernier caliper which was fitted locally on the fixed vertical stand and with the stand of the rotating stage of the microscope so that a relative height of the objective with respect to the plane of the specimen could be measured. Any variation in the focal plane of the specimen could be easily traced with this adjustment. The height has been measured keeping the focus of the objective on the singularity point of the FCD which is the end of the hyperbola curve formed by the singularity of the smectic layers at the air-FLC interface. The nature of curvature is found to be circular, Fig. 2. The experimental data of height measurement of the air-FLC interface are fitted by using the relation

$$R^2 = (\text{Height})^2 + (\text{Spatial distance})^2, \quad (1)$$

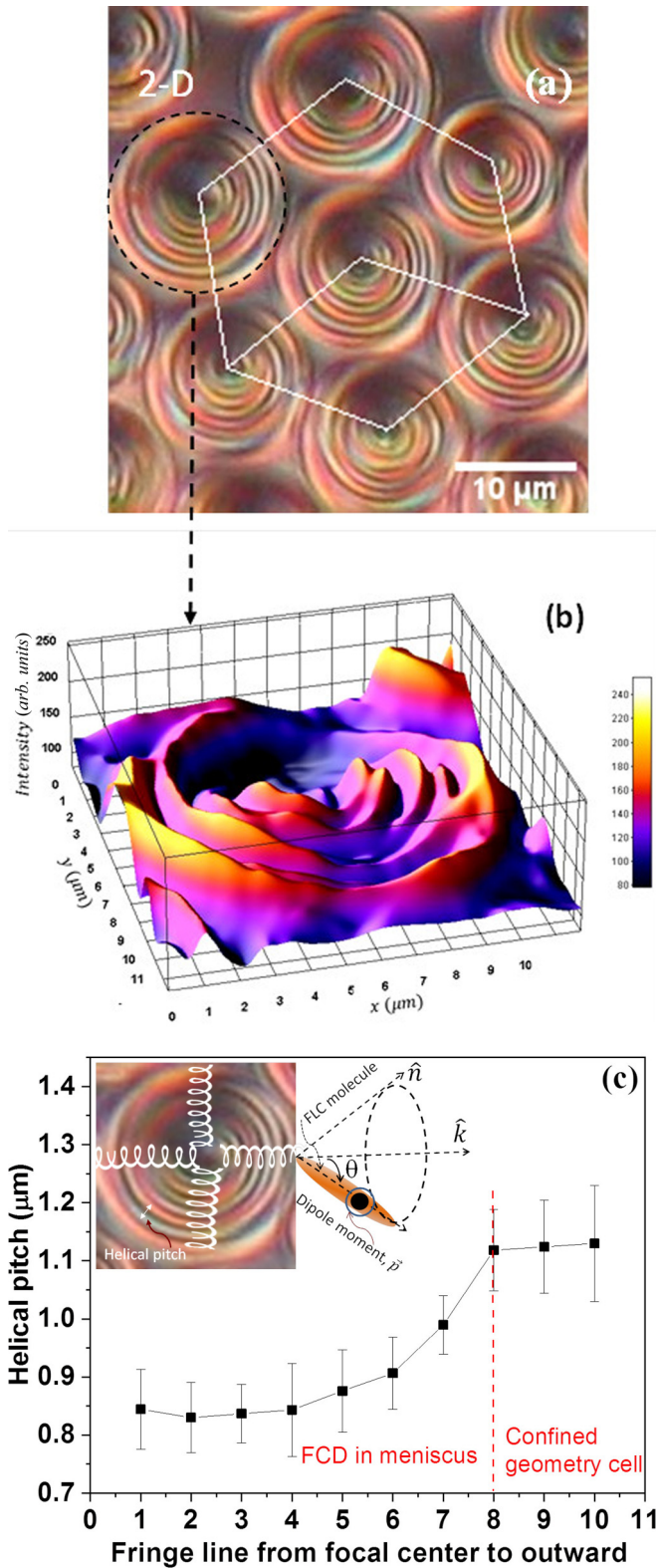


FIG. 3. (a) Localized microscopic optical image of the physical cavity in the middle portion of the meniscus (scale bar $10 \mu\text{m}$) showing a hexagonal pattern; (b) light intensity profile of 3D patterning of one of the FCDs as marked in (a). Intensity profile plotted by using the image analysis tool in IMAGEJ software, where the x - y axes represent the distance in micrometers and the z axis represents the light intensity (arbitrary units). Color variation in the intensity profile indicates the fringe pattern in the meniscus generated by

where R is the radius of curvature of the air-FLC interface and is estimated as $\sim 350 \mu\text{m}$. *Spatial distance* is the physical distance considered within the meniscus from the middle (initial point) to the wall. The FLC film thickness in the middle of the meniscus is around $5\text{--}8 \mu\text{m}$. The height measured directly may not be the exact height of the air-FLC interface touching the wall of the cavity. Therefore, from the experimental data of the contact angle, the height versus spatial distance, one can estimate the exact height of the FLC raised along the wall at the wall-FLC interface by using the Wilhelmy method as $h = \sqrt{2}l^{-1}(1 - \sin \theta_E)^{1/2}$, where θ_E is the contact angle measured at the extreme position (very close to the wall) of the fluid (FLC) near the wall. $l(=\sqrt{g\Delta\rho/\gamma})$ is sometimes also called the capillary constant. Here, $g(=9.8 \text{ m/s}^2)$, $\Delta\rho = \rho_{\text{glass}} - \rho_{\text{liquid crystal}}$, and γ ($\approx 2.3 \text{ mN/m}$) are the acceleration due to gravity, difference between the mass density of glass and the LC, and the interfacial tension of the smectic LC phase, respectively [33–36]. ρ_{glass} and $\rho_{\text{liquid crystal}}$ are the mass densities of glass and the liquid crystal, respectively. The values taken for estimation are comparable to typical values of thermotropic liquid crystals. In the present case, θ_E is calculated as $\sim 24^\circ$ at the extreme position of the meniscus near the wall corresponding to which the height attained by the air-FLC interface touching the wall is $\sim 363 \mu\text{m}$. The direct measurement shows a $\sim 225 \mu\text{m}$ height but the height calculated by the Wilhelmy method is $\sim 363 \mu\text{m}$. The difference is due to the fact that the boundary wall is slightly away from our experimental measurement where the FCDs are not recognizable at the exact boundary of the air-FLC interface touching the wall. The optical region at this exact interface is dark due of light diversion by the interface boundary and hence there is no sufficient transmission through this portion of the sample to focus at the exact boundary. On the other hand, the Wilhelmy method extrapolates the height to the exact level of the air-FLC interface with the cavity wall.

B. Physical structure analysis of FCDs

Figure 3(a) shows the hexagonal self-assembly of FCDs in a two-dimensional optical microscopic image of the middle portion of the meniscus, Fig. 1(b). The prima facie textural observation of the FCD shows that it is a toric FCD [37]. The average diameter of the shown FCDs is around $13.4 \mu\text{m}$ and the average peripheral dimension of the hexagon is around $14.3 \mu\text{m}$. The angles between adjacent axes of the unit cell are $\sim 58^\circ$ and $\sim 122^\circ$. However, these parameters are not fixed throughout the sample but they go on changing due to the variation in the height of the air-FLC material from the middle of the meniscus to the wall of the cavity. Figure 3(b) shows the three-dimensional (3D) intensity profile of one FCD, with the *singularity* point as the dark spot which is not exactly at the center of the base circle. The profile is generated by

helical molecular orientation by successive smectic layers, and (c) helical pitch value calculated by measuring the distance between the two dark or two bright lines of eight lines from the center outward in each of nine FCDs in the texture of Fig. 1(b) and in planar confined geometry cell texture in Fig. 1(c); averaging and deviation are calculated by the standard deviation method of collected data.

image analysis tool IMAGEJ. The dark spot of the FCD is the singularity point. The location of this spot can be roughly estimated by heating the sample to the SmA^* phase where SmC^* dechiralization lines disappear and a clear view of the singularity point can be seen. This is due to the fact that the apparent difference between the two smectic phases is the dechiralization lines. The disappearance of these lines does not affect the smectic layers wrapping about the ellipse and hyperbola in the FCD structure to a large extent. Hence, the singularity point is supposed to be at the same spatial location in the texture in both the SmC^* and SmA^* phases. This equivalence of singularity point in both phases is expected to be the same in every portion of the meniscus (in the center as well as near the walls). After cooling the sample to the SmC^* phase this exact point becomes dark due to the molecular alignment singularity. Continuous periodic concentric fringe lines around this dark spot can be clearly seen in the FCD due to the interference of light. These concentric fringes in FCDs resemble the dechiralization lines in the confined sample cell of the FLC material [38]. Apart from planar geometry, such dechiralization lines are observed in spherical geometry also [39,40]. Dechiralization lines in FCD with concentric rings indicate the formation of helical structure by a curved smectic layer; this requires further analysis of the helical pitch of the molecular director in successive smectic layers, as discussed below.

Figure 3(c) shows the measurement of the gap between the two dark or two bright fringes in the FCD structure and compares them with the planar confined geometry in the same sample. This gap is called the helical pitch of the molecular director of the FLC material. The pitch in the FCD is less than the pitch in the planar confined geometry. The pitch value in the planar confined geometry between the bottom and top substrates [Fig. 1(c)] is around $\sim 1.1 \mu\text{m}$ in this FLC material. Its interpretation can be speculated owing to the aspect of smectic layers that the wrapping of the smectic layers in the chiral phase induces a larger phase angle between successive smectic layers which would allow the molecular director to complete a cycle faster than in confined geometry. The completion of a helical cycle in the FCD will be faster than in confined geometry which has shortened the pitch. However, in the confined geometry, the molecular tilt angle is still maintained with the natural helical structure which means the molecular director and its associated dipoles are continuously rotating in successive smectic layers about the pseudohelical cone.

The FCDs are self-assembled hierarchically in the meniscus but there is a gradual change in the size and shape of FCDs from the middle to the walls due to varying layer thickness of the FLC material in the meniscus, as shown in Fig. 4. Three localized regions in the meniscus, two near the opposite boundary walls and another at the middle of the meniscus, are investigated for the analysis of the FCD structure. In the central region of the meniscus (top inset of Fig. 4), the FCDs are self-assembled as also shown in Fig. 3. The periodic appearance of the singularity point of the FCD as a function of the height of the meniscus is found to be proportional to the height of the meniscus [41]. In the middle of the meniscus and parallel to the length of the meniscus, the FLC film thickness is very thin, $\sim 5 \mu\text{m}$ (Fig. 2). The interfacial boundary between

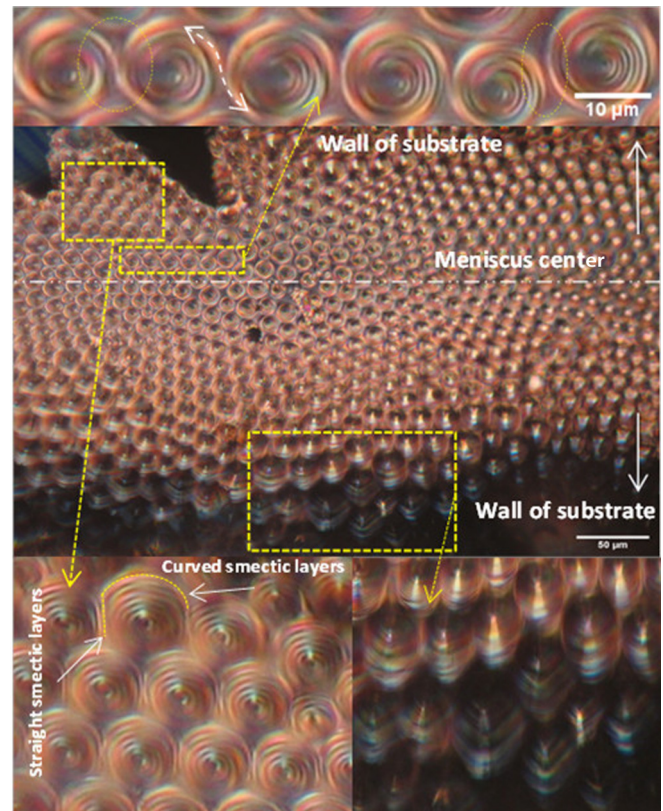


FIG. 4. Cross polarized optical micrograph of the texture of the FLC meniscus. The central part of the figure indicates the complete patterning of FCDs in the meniscus. Scale bar $50 \mu\text{m}$. In the top portion, a layers-unwrapping-like phenomenon takes place via connecting the outermost helical structure of two neighboring FCDs. Scale $10 \mu\text{m}$. Bottom-right image indicates the curved and straight interface of two FCDs whereas the bottom-left portion shows the FCDs with larger size.

the two adjacent FCDs is realized as a bridge between two FCDs at this thickness. However, this has not been revealed in every pair. We interpret this as the wrapping of the helical structure from one FCD to another. Since the helical structure is formed by the molecular director in successive layers and the linkage shown between two FCDs is a part of this helix, therefore it could be indirectly inferred that the wrapping of the helical structure is associated with the orientation of the smectic layers. This might be due to the reason that the outer boundaries of the two FCDs interfere with each other to minimize the interaction energies and result in the redistribution of the molecular alignment.

The FCDs near the walls of the substrate are shown in the enlarged insets at the bottom of Fig. 4. The interface of two FCDs in the bottom left inset of Fig. 4 shows that the helical structure of nearby FCDs is restricted to a line due to the expansion of the size of the FCDs and verifies the *law of impenetrability* of two nearby FCDs by forming a tangential interface [18]. This limitation suppresses the smectic layers' curvature to tangential and hence dechiralization lines are also modified to the tangent lines.

The singularity point of the FCD near the cavity wall is observed very far from the center of the FCD and is larger than

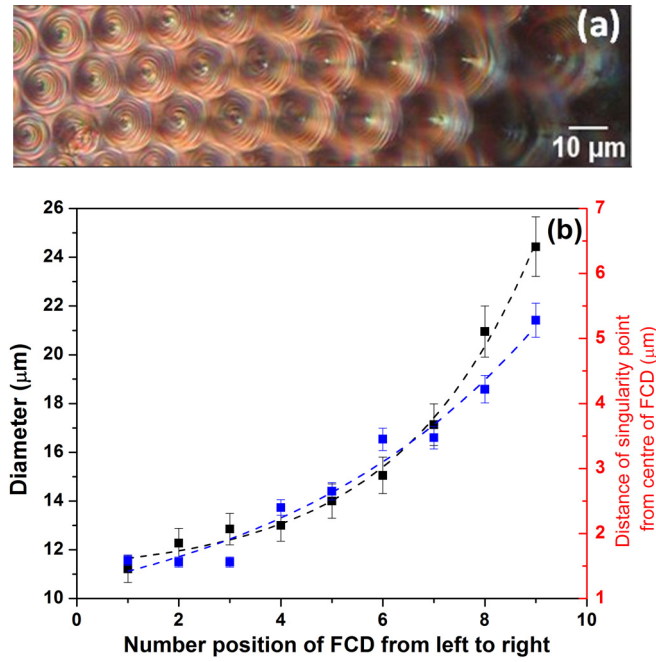


FIG. 5. Physical analysis of FCDs performed by measuring the singularity point from the center of the FCD. (a) Half portion of the meniscus from the center toward the walls; having a total of nine FCDs for the analysis from left to right, scale bar $10\ \mu\text{m}$ and (b) diameter of the viewed FCD and the singularity point from the viewed central portion of the FCD. The dashed lines in both curves show exponential fitting.

any other region in the middle of the meniscus. The singularity point of the FCD exhibits the tilting toward the midline of the meniscus. Consequently, it can be inferred that the singularity point of the FCD is directed toward the air-FLC interface. The possibility of adopting the *law of corresponding cones* by adjacent FCDs is ruled out due to the fact that the tilting of the singularity point is not toward the adjacent FCDs but toward the air-FLC interface [18]. This means that the singularity point is not exactly at the center of the FCD but varies with film thickness near the boundary walls.

For the qualitative analysis of the packing in the middle of and near the wall of the meniscus, the observed textures are roughly assumed as circular. However, they are elliptical if three-dimensional structure is considered, as discussed later in the text. The texture of Fig. 5(a) is used to calculate the variation in the diameter and position of the singularity point from the center of the FCDs with spatial distance from the middle to the wall. A total of nine FCDs in a row from left to right are considered for calculation. The extreme left part of the texture is in the middle of the meniscus whereas the extreme right part is near the wall. The calculation is done by using the image analysis tools by drawing a circle over the FCD and finding the distance of the singularity point from the center. The variation of diameter and singularity point of the FCDs increases nonlinearly (exponential) from left to right in the texture, Fig. 5(b). As the FLC film thickness increases from the middle to the wall, the FCD gets a larger space to expand more than in the middle region; hence the diameter increases. On the other hand, the air-FLC interface contains the

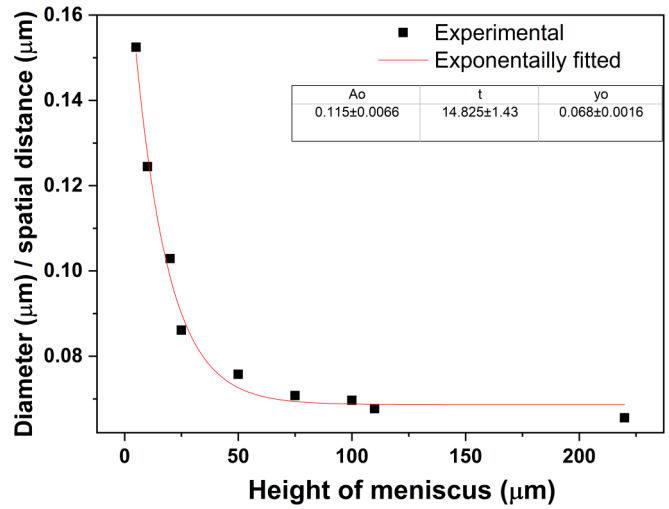


FIG. 6. Estimation of the ratio of the diameter (in μm) to the spatial distance from the center toward the walls where the height (in μm) of the interface also increases. Data are fitted using several iterations of the exponential method, $y = A_0 \exp\{-\frac{x}{t}\} + y_0$, where A_0 is the value of the ratio at $x = 0$, y represents the ratio of diameter to spatial distance, x represents the height, t is the decay constant, and y_0 is the offset value of the ratio at larger height. Values of fitted parameters are given in the graphs.

end of the hyperbola singularity as a dark spot, i.e., singularity point. The height variation of the air-FLC interface allows the deviation of the singularity point from the center of the FCD in the meniscus region near the wall. The larger deviation makes the FCDs more asymmetric near the wall than in the middle region, giving rise to hexagonal tilting structures close to the walls of the meniscus, Fig. 5(b).

The size of the FCDs is found to be increasing from the middle of the meniscus to the physical cavity wall; therefore, the structure is supposed to vary with the height of the air-FLC interface due to a change in the volume of the FCD. The size of the FCD is estimated by the base radius equation as $r_{\text{base}} = h \tan(\omega)$, where ω and h are the angle between the slant height from the singularity point to the base circumference and the vertical height of the FLC film, respectively [37]. The base radius is taken from the data of the diameter and the height is taken from the air-FLC interface to calculate the angle ω . The measure of ω is the estimating parameter for the physical size of the FCD [37]. In the middle of the meniscus, the size estimating parameter ω is calculated as $\sim 47.8^\circ$ ($r_{\text{base}} \approx h$) which later decreases to $\sim 3^\circ$ ($r_{\text{base}} \ll h$) toward the cavity walls. In the middles of the meniscus, h is $5\ \mu\text{m}$ (Fig. 2) and r_{base} is $5.5\ \mu\text{m}$ (Fig. 5) whereas near the wall, h is $250\ \mu\text{m}$ (Fig. 2) and r_{base} is $13\ \mu\text{m}$ (Fig. 5). Thus the value has shown an increase in size. The size of the FCD estimation is further analyzed by physical parameters as the diameter of FCD, spatial distance, and height of the FLC film in the meniscus. The compilation of the three parameters is done by measuring the ratio between the diameter of the FCD and the spatial distance which is analyzed as a function of the height of the film, Fig. 6. Height and spatial distance are circularly related, as shown in Fig. 2. However, the diameter has an exponential relation with respect to spatial distance

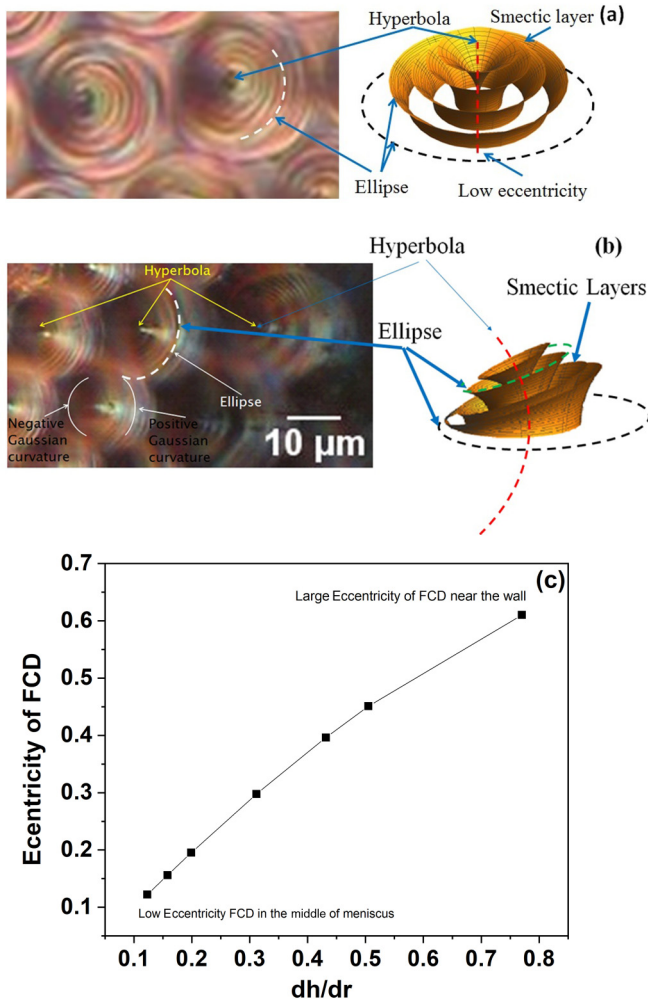


FIG. 7. (a) Optical texture of FCD in the middle of the meniscus and its correlation with the schematic, (b) optical texture of the FCD near the wall and its correlation with the schematic, and (c) eccentricity of the FCD as a function of the slope of the meniscus of the air-FLC interface estimated by using experimental data from Fig. 2; it exhibits the large ellipse nature near the wall of the physical cavity.

and height, Fig. 6. The decay of the ratio is exponential as seen in Fig. 6. In conclusion, the ratio has not shown the same behavior as the air-FLC interface curvature.

The height of the FCDs varies circularly from the middle toward both walls due to the air-FLC interface. This leads to the nonlinear behavior of the shift in the singularity point from the center of the FCD, resulting in the change in the eccentricity of the FCD also. It is significant to identify the hyperbola and ellipse in FCDs before calculating the eccentricity. Figure 7(a) correlates the optical texture in the middle portion of the meniscus with the schematic drawn using the equation for the Dupin cyclide [18]. The end of the hyperbola lies in the dark spot of the FCD whereas the smectic layers wrap along the ellipse. The shape of the FCD is nearly circular with low eccentricity. Similarly, Fig. 7(b) qualitatively correlates the optical texture of FCDs near the wall with the schematic. The tilting of the dark spot (end of hyperbola) away from the center indicates the larger eccentricity than in the middle of

the meniscus. This means that the eccentricity varies with the slope of the air-FLC interface. Thus, the calculation of the eccentricity of the FCD with the air-FLC interface, having nonzero curvature, is estimated by using the equation $e^2 = (dh/dr)^2 / [1 + (dh/dr)^2]$, where h is the height and r is the spatial location to measure the slope (dh/dr) at the interfacial curve [15]. The slope of the interface with nonzero curvature is calculated using the data of height and spatial distance, Fig. 2, from the middle toward the wall of the cavity. The estimated eccentricity of the FCD as a function of slope of the air-FLC interface is nonlinear as shown in Fig. 7(c). The low value of eccentricity shows the shape of the FCD as nearly circular and its large value near the wall shows a largely tilted FCD.

Free energy expression for the FCD is estimated as the combination of three basic contributions. Two contributions are the same as reported earlier [18,42]: $f_{total} = f_{core} + f_{bulk} + f_{SmC^*}$, where *total*, *core*, *bulk*, and *chiral smectic C phase* are the terms used in a combination from various contributions, the inner portion of the FCD near the singular line, the topological and curved nature of smectic layers due to wrapping around the singularity line, and the orientation of the FLC molecular director in successive layers in a helical manner, respectively. Here, $f_{bulk} = f_{topology} + f_{curve}$; $f_{topology} = -4\pi \Lambda a(1 - e^2)K(e^2)$ where $\Lambda = 2K_1 + \bar{K}$; K and \bar{K} are the splay and saddle-splay elastic constants, respectively. “ a ” is the semimajor axis. The minus sign is the signature of negative Gaussian curvature formed by smectic layers. $f_{curve} = -4\pi K_1 a(1 - e^2)K(e^2) \ln \frac{2b}{r_c}$, where b , K , and r_c are the semiminor axis, elliptical integral of the first kind, and core radius, respectively [18]. It is assumed for simplicity that $r_c \approx \sqrt{K_1/B}$ will remain almost a constant along the ellipse and the core free energy will be K_1 per unit length along the ellipse in the middle of the meniscus where the point of hyperbola (cusp of FCD) lies on the plane of FCD. As the meniscus film thickness increases, the cusp of the FCD moves away from the plane of the FCD due to which the core free energy decreases. The core energy can be taken as $f_{core} = 8aK_1E(e^2)$ [18]. Here, “ B ” is the modulus of compressibility. “ E ” is the complete elliptical integral of the second kind.

As noticed in the FCD textures, the consideration of the free energy function (f_{SmC^*}) of the FLC is due to the helical structure formation of the molecular director. However, it has been theoretically estimated that the free energy for curved smectic layers in the SmA phase is persistent with constant layer spacing [43]. The free energy estimation of the SmC film in the meniscus has recently been carried out by Madhusudana [41]. The tilt projection vector \mathbf{c} of the polarization vector in the smectic layer surface allows the distortion of the smectic layer as $\mathbf{c} \times \text{curl}$ [41], which was considered for the stripe domains profile of the smectic layer. In the SmC phase, the polarization vector is easy to visualize theoretically but in the SmC* phase it becomes rather complicated due to the presence of the chirality of the FLC molecules. As the smectic layers are wrapped in the FCD in SmC*, the associated polarization vector is radially outward and generates the energy which is minimized by the helical structure formation. This profile complicates the theoretical calculation and needs a dedicated analysis which is not considered for further analysis in this article.

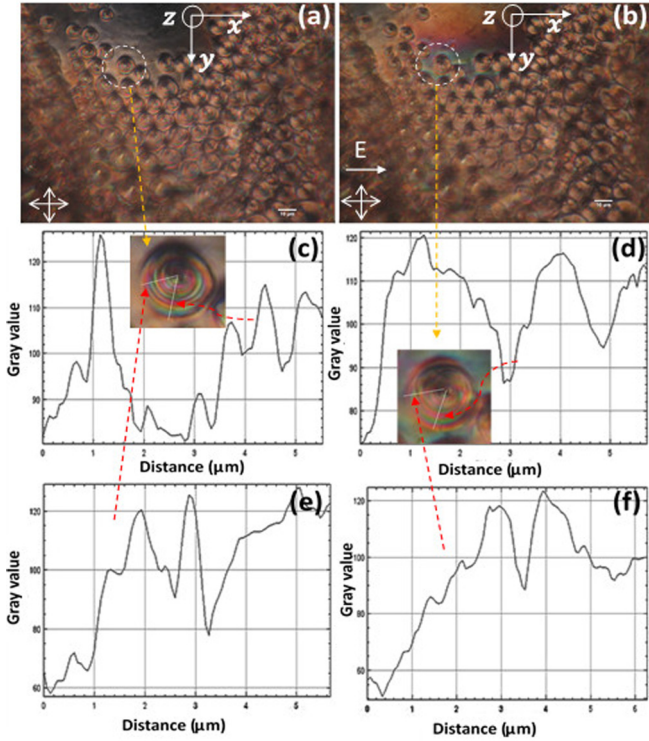


FIG. 8. Optical texture of FCDs in the meniscus at (a) 0 V and (b) 30 V applied bias voltage. Profile of the texture of the FCD in the inset under the line drawn from the center downward (y axis) at (c) 0 V and (d) 30 V. Profile of the texture in the inset under the line drawn from the center to the left side (x axis) at (e) 0 V and (f) 30 V applied bias voltage. Scale bar is $10 \mu\text{m}$.

C. Effect of electric field

Application of an electric field has shown remarkable size variation [44] and induction of large eccentricity of FCDs in the SmA phase [45]. In normal conditions, when a field is applied on a FLC system, the helix gets unwound due to the application of electric torque on the molecular dipoles in the helical structure [46]. Since the FLC is tilted and in the chiral smectic C phase, it is interesting to examine the intrinsic helical structure persisting inside the FCD. The observation of a fine textural line in the FCD indicates the helical structure formation and can be confirmed by applying an electric field.

In order to verify our results, we further investigated the molecular response of the FCDs and helical structures in the meniscus geometry by applying an electric field. The electric field is applied in plane with the ITO electrodes designed on the substrate with the mutual separation of $\sim 200 \mu\text{m}$. The gap between the electrodes is positioned so that the cavity could lie over this gap and an electric field could be applied on the material in the cavity. As can be seen in Fig. 8, the FCD textures at 0 V [Fig. 8(a)] and 30 V [Fig. 8(b)] dc voltages are recorded for the confirmation of helical structure formation and its unwinding process. The gap between two plane electrodes is $\sim 200 \mu\text{m}$; therefore, an electric field of $0.15 \text{ V}/\mu\text{m}$ on the bulk is sufficient for unwinding the helix and not for distorting the smectic layers. Indeed, an asymmetrical dis-

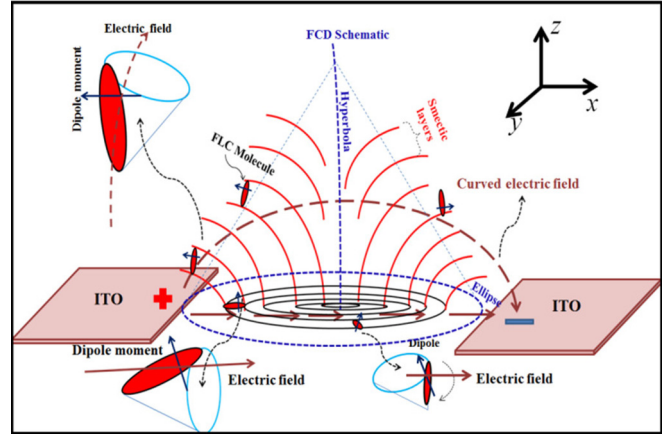


FIG. 9. Schematic of FCD between the two in-plane electrodes and their associated electric field lines as per the given polarity. FLC molecules aligned radially in the smectic layers and response to the electric field by rotating about the surface of the pseudocone structure. Schematic of smectic layers showing the wrapping of layers about the ellipse and hyperbola which are the basic structure of FCDs. The structure in the schematic is not to scale.

ortion of the FCD structure is observed at 30 V dc bias, as shown in Fig. 8(b). The torque experienced by the molecules is $\tau = \vec{p} \times \vec{E}$, where \vec{p} is the dipole moment associated with the FLC molecules and \vec{E} is the applied electric field which is nonuniform throughout the FCD due to its curved nature. As per the shape, one portion is supposed to experience greater torque as compared with another portion. This is because the angle formed by the FLC molecule with the electric field pointing in plane is varying from 0° to 90° in one-quarter of 360° around the FCD at the portion near the interface with the substrate, resulting in the nonuniform helical unwinding with *in-plane* electric field as seen in Figs. 8(c) and 8(d).

The application of an electric field on the sample by the in-plane electrodes is sketched in the schematic of Fig. 9. The molecular alignment of FLC in the cavity is not planar throughout the sample but it has planar alignment at the aligning substrate and vertical at the air-FLC interface. In the middle of the bulk, the alignment is varying from planar to perpendicular due to which the electric field exposure is also nonuniform. Besides the planar and vertical alignment, the molecules are in smectic layers which are in FCD form. This is again a region of non-uniform electric field. Further, the electric field itself is nonuniform as shown in the schematic in Fig. 9. The strength of the electric field to unwind the helical structure can be estimated by knowing the critical electric field value [47], $E_c \approx Kq_0^2\theta^2/P \approx 0.102 \text{ V}/\mu\text{m}$, where K is the elastic constant (one-constant approximation, typical value $\sim 5 \times 10^{-12} \text{ N}$) [48]; $q_0(=2\pi/p_0)$ is the wave vector of the helix, where p_0 is the pitch value of FLC. $\theta(\sim 21^\circ)$ is the tilt angle of the molecular director, n , from smectic layer normal. Basically, there are two main regions of large asymmetric switching; one is along the x axis and another is along the y axis, Fig. 9. Molecules in the x -axis region are aligned with the electric field but their dipoles have a nonzero angle with it at the substrate interface. However, in the same orientation

at some distance along the z axis, the alignment of FLC molecules and their dipoles becomes nonzero which causes them to switch less than the molecules along the y axis. The same observation is in agreement with experimental findings as well.

In Fig. 8(a), there is a formation of helical structure in the absence of electric field as indicated by the observation of dechiralization lines. As a voltage of 30 V is applied, Fig. 8(b), the unwinding of the helical structure results due to a $0.15 \text{ V}/\mu\text{m}$ electric field. Since the helical formation is formed in 3D spherical symmetry, there will evolve *two types of structural changes* under the application of electric field; one is that in which smectic layers are perpendicular (x axis) to the applied field and the second is that in which they are parallel (y axis). The structure change will be large for the perpendicular smectic layer structure whereas it will be less for parallel. This happens because of the application of an electric field at different angles in each configuration. Such textural changes are indicated by the disappearance of dechiralization lines. Intrinsic shape and transmission color through FCD, encircled in Figs. 8(a) and 8(b), has not changed but only the helical lines have disappeared, suggesting the nondistortion of smectic layers. For the realization of appearance and disappearance of dechiralization lines by an electric field, an intensity profile is plotted across the marked lines of the FCD images in the inset of Figs. 8(c) and 8(d). In Figs. 8(c) and 8(d), the profiles show the helical structure under the line drawn along the y axis in the absence and presence of an electric field, respectively, whereas Figs. 8(e) and 8(f) exhibit the profile under the line drawn along the x axis in the absence and presence of an applied electric field, respectively. As discussed earlier, each FCD corresponds to possess a complete helix formation in FLC, thereby implying that the helix is distorting with greater magnitude in the region perpendicular to the applied electric field (y axis) whereas it has weak distortion in the direction along to it (x axis). Considering the point of maximum distortion in the line drawn along the y axis, we can assume that molecules are perpendicular to the applied field whereas the molecular direction in the line drawn along the x axis is parallel to the field. The application of an electric field along the y axis generates a torque on the molecular dipole which results in the molecules rotating about the surface of a pseudocone, Figs. 8(b), 8(d), and 9. On the other hand, in the line along the x axis, where the molecules are parallel to the applied field, but dipoles are still perpendicular to the direction of the applied field, Figs. 8(b), 8(f), and 9, the dipolar rotation is shorter than the molecules along the y axis. This minute switching in the latter case, Fig. 8(f), is not allowing the line profiles in Figs. 8(e) and 8(f) to be the same. This molecular arrangement of under the line profile is causing the asymmetric helical unwinding, as shown in Fig. 8 and the schematic in Fig. 9.

D. Effect of temperature

The presence of helical structure in a FCD is further confirmed by the temperature dependent studies as shown in Fig. 10, where the presence of helical structure in the deep SmC^* phase could be clearly realized through optical textures. Such optical textures were recorded under a cross polarizer

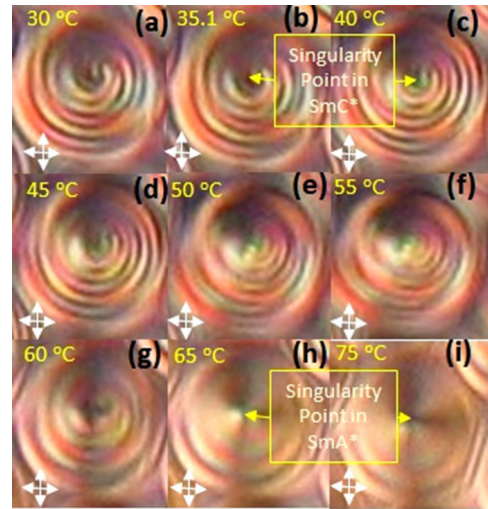


FIG. 10. Temperature dependent variations in FCD: (a) 30 °C, (b) 35.1 °C, (c) 40 °C, (d) 45 °C, (e) 50 °C, (f) 55 °C, (g) 60 °C, (h) 65 °C, and (i) 75 °C. Crossed arrows indicate the position of the polarizer and analyzer.

ing microscope. The required temperature was controlled by using a high precision temperature controller. As seen in Fig. 10(a), it has been observed that the dechiralization lines persist in the temperature range 30 °C–55 °C, where the FLC material is in the SmC^* phase. At 60 °C, the dechiralization lines begin to blur, suggesting the unwinding of helical structure and the disappearance of the tilt angle of the molecular director in smectic layers. This behavior is the same as in bulk FLC materials. Finally, the dechiralization lines disappeared after the transition temperature (66.4 °C) which verifies the SmA phase of the material. We have observed circular color contrast but no distinct fringes for temperature 65 °C–75 °C. Here, it is important to notice that the dark portion at the center of the FCD in the SmA^* phase becomes a very sharp point which is considered as the singularity point of the FCD in SmC^* and the end point of the hyperbola passing through the ellipse of it.

IV. CONCLUSION

FLC material in the SmC^* phase has shown a hierarchical assembly of focal conic domains (FCDs) in the meniscus of the physical cavity. It is found to be circular in the meniscus and air-FLC interface according to which the size and shape of FCDs is self-arranged. These FCDs are formed by balancing of energies among the anchored LC molecules at the interface of the substrate, distortion of smectic layers, and surface tension. However, larger FCDs are formed near the boundary walls whereas they are smaller in the center of the physical cavity. In all the FCDs, concentric, but some broken rings are observed and analyzed in the SmC^* phase. The disappearance of rings by applying a dc electric field and for higher temperature dependent studies have confirmed that these rings are helical structure based dechiralization rings and observed in the FCDs in the meniscus geometry of FLC. Furthermore, on the basis of optical analysis, the central part of the meniscus possessed a hexagonal periodic pattern which is lost as the

cavity boundary is approached due to varying size of FCDs and FLC film thickness. A phenomenon of unwrapping the helical structure from one and wrapping on the other FCD is also observed in the middle of the meniscus. If the physical parameters such as spacing, size, FLC film thickness, etc., are changed, the interface would also be distinct. For example, if the FCDs are small and spacing is large, the isolated FCDs are clearly observed, but if the spacing is short and size is large, the tangential interface is formed between two FCDs. This is an indication of the suppression of a curved smectic layer forming the helical structure into a flat one. The FCD formation and the understanding of the helical structure in it are significant for their application in microlenses and optical components.

ACKNOWLEDGMENTS

We sincerely thank Professor Venu Gopal Achanta, Director, National Physical Laboratory, New Delhi for his continuous encouragement in the work. The authors sincerely thank the late Professor W. Haase, Germany, for providing the FLC material. A.C. is thankful to Professor Rajiv Aggarwal, Principal, Deshbandhu College (University of Delhi), New Delhi for the encouragement for this activity. We are thankful to the referees also for useful suggestions to make the findings more informative. A.M.B. and A.B. are thankful to Council of Scientific and Industrial Research (CSIR), India. Grant Number is [21(986)/13/EMR-II], New Delhi for financial assistance under the emeritus and SRF-fellowship schemes, respectively.

-
- [1] J. S. Rowlinson and B. Widom, *Molecular Theory of Capillarity* (Dover Publications, Mineola, NY, 1984).
- [2] J. C. Loudet, P. V. Dolganov, P. Patrício, H. Saadaoui, and P. Cluzeau, *Phys. Rev. Lett.* **106**, 117802 (2011).
- [3] M. Selmi, J.-C. Loudet, P. V. Dolganov, T. Othman, and P. Cluzeau, *Soft Matter* **13**, 3649 (2017).
- [4] K. Harth, B. Schulz, C. Bahr, and R. Stannarius, *Soft Matter* **7**, 7103 (2011).
- [5] G. Friedel, *Ann. Phys. (Paris)* **9**, 273 (1922).
- [6] W. Bragg, *Nature (London)* **133**, 445 (1934).
- [7] J. P. Sethna and M. Kléman, *Phys. Rev. A* **26**, 3037 (1982).
- [8] Y. H. Kim, D. K. Yoon, H. S. Jeong, O. D. Lavrentovich, and H.-T. Jung, *Adv. Funct. Mater.* **21**, 610 (2011).
- [9] J. P. Bramble, S. D. Evans, J. R. Henderson, T. J. Atherton, and N. J. Smith, *Liq. Cryst.* **34**, 1137 (2007).
- [10] B. Zappone, C. Meyer, L. Bruno, and E. Lacaze, *Soft Matter* **8**, 4318 (2012).
- [11] R. S. Preusse, E. R. George, S. A. Aghvami, T. M. Otchy, and M. A. Gharbi, *Soft Matter* **16**, 8352 (2020).
- [12] S. Shojaei-Zadeh and S. L. Anna, *Langmuir* **22**, 9986 (2006).
- [13] A. Honglawan, D. A. Beller, M. Cavallaro, R. D. Kamien, K. J. Stebe, and S. Yang, *Proc. Natl. Acad. Sci. USA* **110**, 34 (2013).
- [14] M. C. Choi, T. Pfohl, Z. Wen, Y. Li, M. W. Kim, J. N. Israelachvili, and C. R. Safinya, *Proc. Natl. Acad. Sci. USA* **101**, 17340 (2004).
- [15] D. A. Beller, M. A. Gharbi, A. Honglawan, K. J. Stebe, S. Yang, and R. D. Kamien, *Phys. Rev. X* **3**, 041026 (2013).
- [16] M. Kleman and O. D. Lavrentovich, *Soft Matter Physics: An Introduction* (Springer, New York, 2004).
- [17] Y. H. Kim, D. K. Yoon, M. C. Choi, H. S. Jeong, M. W. Kim, O. D. Lavrentovich, and H.-T. Jung, *Langmuir* **25**, 1685 (2009).
- [18] M. Kléman and O. D. Lavrentovich, *Eur. Phys. J. E* **2**, 47 (2000).
- [19] Y. H. Kim, J.-O. Lee, H. S. Jeong, J. H. Kim, E. K. Yoon, D. K. Yoon, J.-B. Yoon, and H.-T. Jung, *Adv. Mater.* **22**, 2416 (2010).
- [20] T. Ohzono, Y. Takenaka, and J. Fukuda, *Soft Matter* **8**, 6438 (2012).
- [21] J. S. Patel and J. W. Goodby, *J. Appl. Phys.* **59**, 2355 (1986).
- [22] A. Fukuda, Y. Ouchi, H. Arai, H. Takano, K. Ishikawa, and H. Takezoe, *Liq. Cryst.* **5**, 1055 (1989).
- [23] K. Nakamura and T. Akahane, *Jpn. J. Appl. Phys.* **29**, L1157 (1990).
- [24] A. Iida and Y. Takanishi, *Liq. Cryst.* **34**, 1285 (2007).
- [25] S. M. Hare, B. Lunsford-Poe, M. Kim, and F. Serra, *Materials (Basel)* **13**, 3761 (2020).
- [26] Y. H. Kim, H. S. Jeong, J. H. Kim, E. K. Yoon, D. K. Yoon, and H.-T. Jung, *J. Mater. Chem.* **20**, 6557 (2010).
- [27] J. H. Kim, Y. H. Kim, H. S. Jeong, M. Srinivasarao, S. D. Hudson, and H.-T. Jung, *RSC Adv.* **2**, 6729 (2012).
- [28] F. Serra, M. A. Gharbi, Y. Luo, I. B. Liu, N. D. Bade, R. D. Kamien, S. Yang, and K. J. Stebe, *Adv. Opt. Mater.* **3**, 1287 (2015).
- [29] D. K. Yoon, M. C. Choi, Y. H. Kim, M. W. Kim, O. D. Lavrentovich, and H.-T. Jung, *Nat. Mater.* **6**, 866 (2007).
- [30] A. Bawa, A. Choudhary, A. K. Thakur, S. Kumar, Rajesh, S. P. Singh, and A. M. Biradar, *Appl. Phys. A* **126**, 171 (2020).
- [31] A. Bawa, L. K. Gangwar, A. Dhingra, A. Choudhary, Rajesh, S. P. Singh, W. Haase, and A. M. Biradar, *Liq. Cryst.* **46**, 166 (2019).
- [32] A. Bawa, A. Choudhary, G. Sharma, Rajesh, S. P. Singh, and A. M. Biradar, *Appl. Surf. Sci.* **526**, 146743 (2020).
- [33] M. Tintaru, R. Moldovan, T. Beica, and S. Frunza, *Liq. Cryst.* **28**, 793 (2001).
- [34] T. F. Tadros, *Basic Principles of Dispersions* (Walter de Gruyter, Berlin, 2017).
- [35] D. C. Giancoli, *Physics: Principles with Applications*, 4th ed. (Prentice Hall, Englewood Cliffs, NJ, 1995).
- [36] P. K. Rai, M. M. Denn, and C. Maldarelli, *Langmuir* **19**, 7370 (2003).
- [37] C. Blanc and M. Kleman, *Phys. Rev. E* **62**, 6739 (2000).
- [38] I. Dierking, *Textures of Liquid Crystals* (Wiley, New York, 2003).
- [39] J. A. Sofi and S. Dhara, *Appl. Phys. Lett.* **114**, 091106 (2019).
- [40] A. Chandran, A. Choudhary, P. Singh, D. Haranath, and A. M. Biradar, *Soft Matter* **11**, 749 (2015).
- [41] N. V. Madhusudana, *Phys. Rev. E* **102**, 032701 (2020).
- [42] T. Akahane and M. Nakagawa, *Jpn. J. Appl. Phys.* **25**, L661 (1986).
- [43] C. D. Santangelo and R. D. Kamien, *Proc. R. Soc. London, Ser. A* **461**, 2911 (2005).

- [44] I. Gryn, E. Lacaze, R. Bartolino, and B. Zappone, *Adv. Funct. Mater.* **25**, 142 (2015).
- [45] A. Suh, H. Ahn, T. J. Shin, and D. K. Yoon, *J. Mater. Chem. C* **7**, 1713 (2019).
- [46] J. Pavel, P. Gisse, H. T. Nguyen, and P. Martinot-Lagarde, *J. Phys. II* **5**, 355 (1995).
- [47] S. T. Lagerwall, *Ferroelectrics* **301**, 15 (2004).
- [48] T. C. Chieu, *J. Appl. Phys.* **64**, 6234 (1988).